Research Article Vol. 30, No. 2 / 17 Jan 2022 / Optics Express 689
Optics EXPRESS

Polarization-modulated grating interferometer by conical diffraction

LIN LIU,[1,2] ZHAOWU LIU,[1] SHAN JIANG,[1] WEI WANG,[1] HONGZHU YU,[1] YANXIU JIANG,[1] AND WENHAO LI[1,*]

[1] *Changchun Institute of Optics, Fine Mechanics and Physics, Chinese Academy of Sciences, Changchun, Jilin 130033, China*
[2] *University of Chinese Academy of Sciences, Beijing 101408, China*
[*] *liwh@ciomp.ac.cn*

Abstract: The grating interferometer in the Littrow configuration uses quarter wave plates (QWPs) to modulate the polarization in the measurement system to determine the autocollimation optical path. Fabrication errors and mounting errors of the QWPs lead to phase changes in the grating interferometer that generate measurement errors. As an alternative, we propose a grating interferometer that produces conical diffraction. Using the grating instead of QWPs to modulate the beam's polarization bypasses this source of error. A 45 mm range experiment was performed that yielded a repeated measurement error of 40 nm. Experiments show that the system has a simple structure and good repeatability and is capable of high-precision displacement measurements.

1. Introduction

As an instrument measuring displacement, the grating interferometer has advantages of high precision, high resolution, and good environmental adaptability. Its areas of applications include semiconductor manufacturing, precision processing, advanced optical component manufacture, and biomedicine [1–8]. The grating interferometer can achieve sub-nanometer accuracy in position measurements, and its environmental requirements are less than those for the laser interferometer.

To achieve a higher resolution, a grating with a greater line density is needed. The incidence of the light in the grating interferometer changes gradually from the vertical to the Littrow incidence [9,10]. With the Littrow incidence, polarized light can be used in measurements to improve energy utilization and contrasts in interference signals. Further research has been performed on various aspects such as optical path innovation, error correction, and integration [11,12]. Hu and colleagues [13] used a spatial separation structure to separate beams of different polarization states and frequency states in the optical path to eliminate nonlinear errors incurred in the processing of optical elements and frequency mixing. Zhang and colleagues [14–16] used the similar structure to measure the interference signal independently and decouple the interference signal to realize measurements in both the X and Z dimensional. Siaudinyte and colleagues [17] developed a reading head using optical fiber coupled to a polarization beam splitter (PBS) and realized displacement measurements employing multiple reading heads. Gao Wei and colleagues [18,19] used a two-dimensional grating to realize three-dimensional displacement measurements with nanometer resolutions.

However, in the Littrow configuration, a quarter wave plate (QWP) is needed to modulate the polarization state of the beam. The QWP is set 45° to the optical axis, and hence both the incident light and diffracted light pass through the QWP twice. The polarization state of the beam changes 90° and the measured beam exits from the other side of the PBS. However, inaccuracies in fabrication and installation of the QWP affect the optical axis and hence the phase of the interference signal that generates measurement error. In studies of a laser interferometer, yaw

#438490 https://doi.org/10.1364/OE.438490
Journal © 2022 Received 28 Jul 2021; revised 6 Nov 2021; accepted 20 Dec 2021; published 3 Jan 2022

Optics EXPRESS

errors and ghost reflections appear with the QWP, both of which produce measurement error [20,21]. Although the principle underlying the grating and laser interferometers are similar, the QWP in the grating interferometer also generates measurement error.

In this paper, a high-precision grating interferometer is proposed that exploits conical diffraction to modulate the beam. A measured beam is incident on the grating surface at specific incident angle and azimuthal angle. Its diffracted light used for the measurement is modulated by the grating and becomes polarized. This measured diffracted light is reflected vertically by a reflector and returned to the grating along the original path to undergo secondary conical diffraction. This second diffracted light propagates along the initial incident path and is emitted from the other side toward the signal processing system through the PBS. The setup for conical diffraction reduces the number of QWPs and eliminates measurement error incurred through errors in manufacturing and installation of the QWPs. Experimental results show that the system has good repeatability and good measurement accuracy after calibration.

2. Measurement principle

2.1. Conical diffraction theory

For a given angle between the cross section of incident beam and the direction of the groove line, the cross section of the diffracted light at each diffraction orders forms another angle with the groove line after being modulated by the grating. At this instant, the diffracted light of each order is separated spatially, producing what is referred to as conical diffraction.

In the setup (Fig. 1), light of wavelength λ is incident on the grating surface at incident polar angle θ and the incident azimuthal angle φ; the grating has a groove depth h, a groove width τ, and grating periodicity Λ. The reflection, modulation, substrate layer, and transmission regions are labeled 1 through 4.

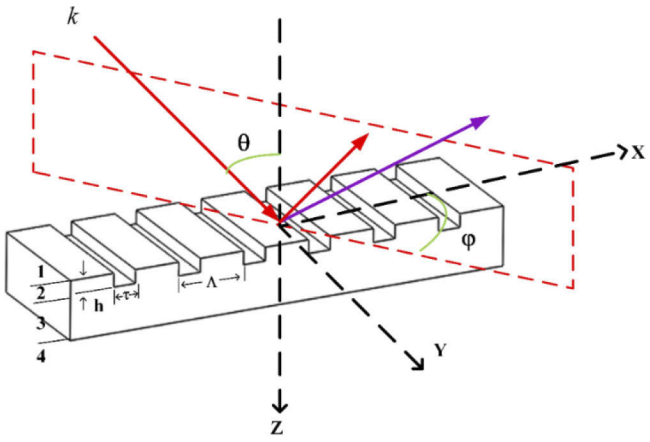

Fig. 1. Schematic of the setup for conical diffraction.

Because the grating is anisotropic in the direction of the groove line and the vertical direction of the groove line, the conical light beam, when incident on the grating, can be regarded as a superposition of P- and S-polarized light that obey a certain geometric relation expressed as the grating equations for conical diffraction [22,23]; specifically,

$$n_l \sin\theta_j \cos\phi_j = \sin\theta\cos\phi + j\frac{\lambda}{\Lambda} \tag{1}$$

$$n_l \sin\theta_j \sin\phi_j = \sin\theta\sin\phi \tag{2}$$

Optics EXPRESS

where j indexes the order of the diffracted light. In accordance with the rigorous coupled-wave analysis (RCWA) [24], the diffraction efficiency for conical diffraction is expressed in the form

$$DE_{rj} = |R_{s,j}|^2 Re(\frac{k_{1,zj}}{k_0 n_1 \cos\theta}) + |R_{p,j}|^2 Re(\frac{k_{1,zj}/{n_1}^2}{k_0 n_1 \cos\theta}) \tag{3}$$

$$DE_{tj} = |T_{s,j}|^2 Re(\frac{k_{3,4,zj}}{k_0 n_1 \cos\theta}) + |T_{p,j}|^2 Re(\frac{k_{3,4,zj}/{n_3}^2}{k_0 n_1 \cos\theta}) \tag{4}$$

which describes diffracted light containing S- and P-polarization components. Because the grating surface has a coating, only the reflection component, Eq. (3), is considered for which $R_{S,\mathrm{j}}$ denotes the S-polarization component of the diffracted light of order j, and $R_{P,j}$ the P-polarization component. The S and P components contain a part of the diffracted light, which is not a line polarization state. Hence, the grating modulates the polarization state of the incident light. The efficiency and phase of the diffracted light in conical diffraction were analyzed. Combined with the polarization produced by PBS, the grating under conical incidence reproduces the effect of a QWP.

2.2. Grating interferometer setup

The setup of the grating interferometer producing conical diffraction is shown in Fig. 2. After passing through the PBS, the laser beam emitted from the laser is divided into transmitted P-polarized light and reflected S-polarized light. Taking the P-polarized light (purple) as an example, the transmitted P-polarized light is incident on the grating via the reflective mirror 2 at an incidence polar angle of 45° and an azimuthal angle of 45°. Subsequently, first-order diffracted light is emitted at a specific azimuthal angle and diffraction angle; the zero-order reflected light is colored blue. The reflective mirror 3 is perpendicular to the first-order diffracted light in purple light, and the second diffracted light returns to the PBS along the incident light path. Because of the modulation function of the grating for conical diffraction, the polarization state of the diffracted light after two diffractions transforms into an elliptically polarized state; hence, part of the diffracted light is reflected by the PBS and sent toward the signal processing system. Similarly, the reflected S-polarized light (marked in red in Fig. 2), diffracts twice along a similar path that changes the polarization state, and is transmitted from the PBS toward the signal processing system. In summary, the two paths followed by the diffracting light beam are (refer to Fig. 2):

Measurement beam (Red): Laser-PBS-RM1-Grating-RM3-Grating-RM1-PBS;
Measurement beam (Purple): Laser-PBS-RM2-Grating-RM4-Grating-RM2-PBS.

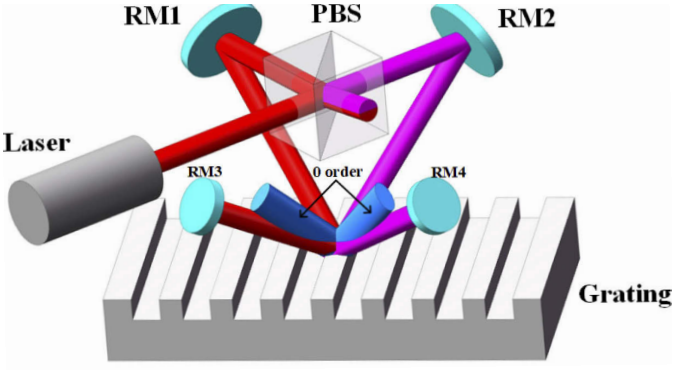

Fig. 2. Grating interferometer setup for conical diffraction (RM: reflective mirror, PBS polarized beam splitter).

Optics EXPRESS

Because the spatial angle of the symmetrically diffracted light is not consistent, combining the two diffracted beams via reflective mirror is difficult. Therefore, reflective mirror 3 and reflective mirror 4 are perpendicular to these symmetrically diffracted lights. The reflected diffracted light becomes the incident light undergoing a second diffraction. The twice-diffracted light propagates along the path of the first incident light and then passes through the PBS from the other side and is sent to the signal processing system.

When the grating moves, the phases of the two measuring beams—here denoted by Φ_1 and Φ_2—change, which from the Doppler shift and grating equations are expressed as:

$$\Phi_1 = 2 \times \frac{4\pi \sin\theta}{\Lambda} \Delta x \tag{5}$$

$$\Phi_2 = 2 \times (-\frac{4\pi \sin\theta}{\Lambda} \Delta x) \tag{6}$$

There are two coefficients in these expressions that arise from the two diffractions that occur in this setup. Moreover, from these expressions, a relation between the phase change in the interference signal and the grating displacement can be obtained; specifically, we have

$$\Delta x = \frac{\Lambda}{8\pi}(\Phi_1 - \Phi_2) \tag{7}$$

That is, after two diffractions, the system realizes a four-fold optical subdivision of the groove width.

3. RCWA simulation

3.1. Diffraction efficiency simulation

The RCWA [25]—a semi-analytical method for solving scattering from periodic structures—is used to analyze the data obtained from various diffraction gratings. The simulation conditions are as follows: the analysis wavelength is 632.8 nm, the polar and azimuthal angles of incidence are both 45°, the aluminum film is plated, and the line density is 1800 gr/mm. The diffraction efficiency of the beam after two diffractions is analyzed. Because the polarization state of the beam changes in conical diffraction, the diffraction efficiency of the P- and S-polarization states need to be calculated after each diffraction, and the diffracted light in conical diffraction includes changes in amplitude and phase. A complex amplitude of the diffracted light after each diffraction is added, and the diffraction efficiency is calculated using the added complex amplitudes. Each component is recorded as DEp-p-p, DEp-p-s, DEp-s-p, DEp-s-s, DEs-p-p, DEs-p-s, DEs-s-p, and DEs-s-s. As an example, DEp-p-p represents the P component of the P-polarized incident light, the first diffracted light, and the second diffracted light. Because the PBS is used for polarization splitting, we need for the interferometry DEp-p-s and DEp-s-s as the S component and DEs-p-p, DEs-s-p as the P component. In actual measurements, these two components need to be consistent to ensure a strong contrast in the interferometry signal.

The results of the analysis are listed in Table 1. After PBS splitting, DEp-p-s and DEs-p-p account for the largest proportion of energy, and their diffraction efficiencies are approximately the same. The contrast in the interference signal received at the receiver is also good. That is, the conical diffraction occurring in the grating acts as a beam polarization modulator.

Given the installation error during assembly, a non-ideal situation is analyzed. Setting the polar and azimuth angles of incidence to between 40–50°, a simulation analysis of each grating type—binary, sinusoidal, trapezoidal, and triangular—is performed. Results are presented in Fig. 3 and Fig. 4.

Besides, we also analysis that duty cycle of grating. Results show as Fig. 5. From figure, though Fig. 5(b), Fig. 5(c) and Fig. 5(d) look like different, the ratio of P-diffraction efficiency

Optics EXPRESS

Table 1. Diffraction efficiency of different polarization states in different grating groove.

Grating type	DE_{p-p-s}	DE_{p-s-s}	DE_{s-p-p}	DE_{s-s-p}
Binary	0.0445	5.0275e-4	0.0446	5.0374e-4
Sinusoidal	0.01472	1.6975e-4	0.0148	1.7157e-4
Triangular	0.0077	7.2934e-5	0.0077	7.2942e-5
Trapezoidal	0.0155	9.1371e-5	0.0155	9.1253e-5

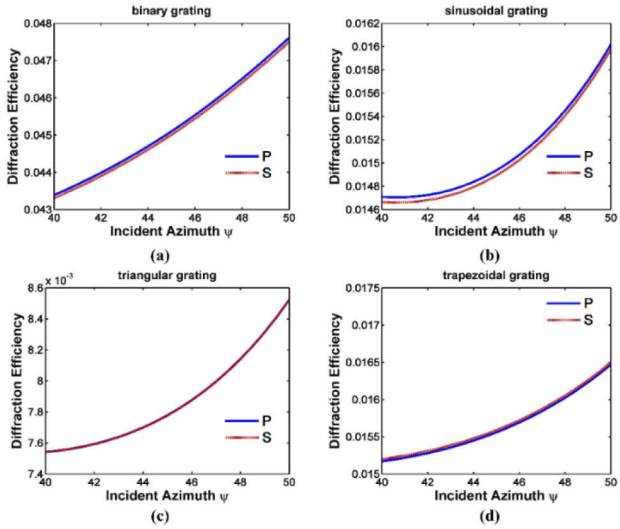

Fig. 3. Dependence of the diffraction efficiency on the azimuthal angle of incidence, for various grating types.

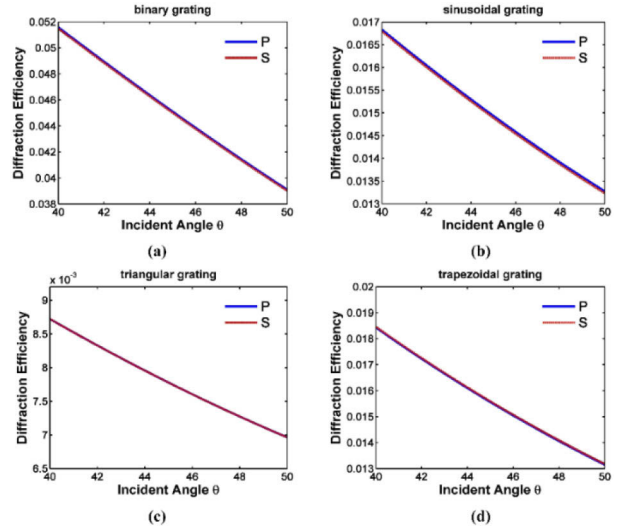

Fig. 4. Dependence of the diffraction efficiency on polar angle of incidence, for various grating types.

Optics EXPRESS

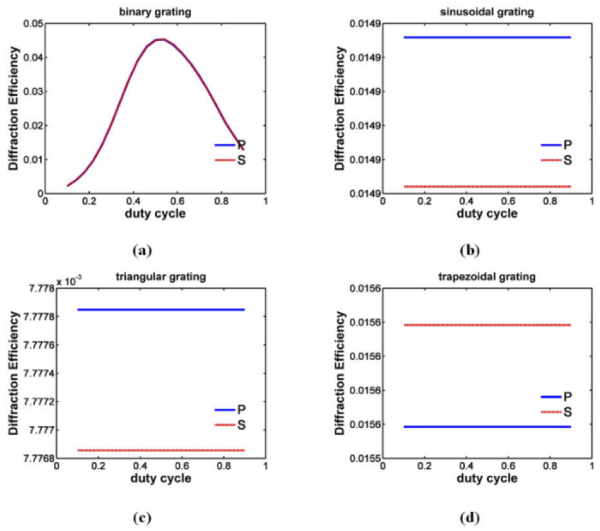

Fig. 5. Dependence of the diffraction efficiency on duty cycle, for various grating types.

and S-diffraction efficiency is near constant. So, duty cycle does not influence the quality of interference signal. Due to this result, the grating parameters can choose for the best diffraction efficiency.

These results of simulation show that when the grating interferometer parameters change, includes incident angle, azimuth angle, duty cycle of grating, the diffraction efficiency also changes. However, the efficiency ratio of the P- and S-polarization states are almost unchanged after the PBS. In this instance, the grating with the higher diffraction efficiency is more advantageous in a measurement system.

3.2. *Workbench error simulation*

When the worktable has pitch (yaw), the incident polar (azimuthal) angle of the grating changes (Fig. 6). Because the polarization state of the grating changes and the phase of the light beam changes in conical diffraction, the phase change induces a change in the incident condition, which in turn affects the accuracy of the interferometry system. To analyze the influence of the installation deviation and table deflection on the system, the influence of deflections and straightness of the table on the conical diffraction measurement system is analyzed. The phase change of the two measuring beams is analyzed by setting the range over which the polar and azimuthal angles of incidence change: specifically, 0–1° in steps of 0.01°. From Section 3.1, the energy of one of the two components of the P or S state is much greater than that of the other, and hence the phase of the component with the higher energy is analyzed.

From Table 2, when the incident angle of the grating changes by 1°, the phase changes by 0.02 rad. Given the relationship between the change in phase and the displacement measurement, the change in displacement is 0.45 nm. When the azimuthal angle of the grating changes, the phase changes by 0.01 rad and the displacement changes by 0.23 nm. The system is less affected by the table pitch and straightness.

Optics EXPRESS

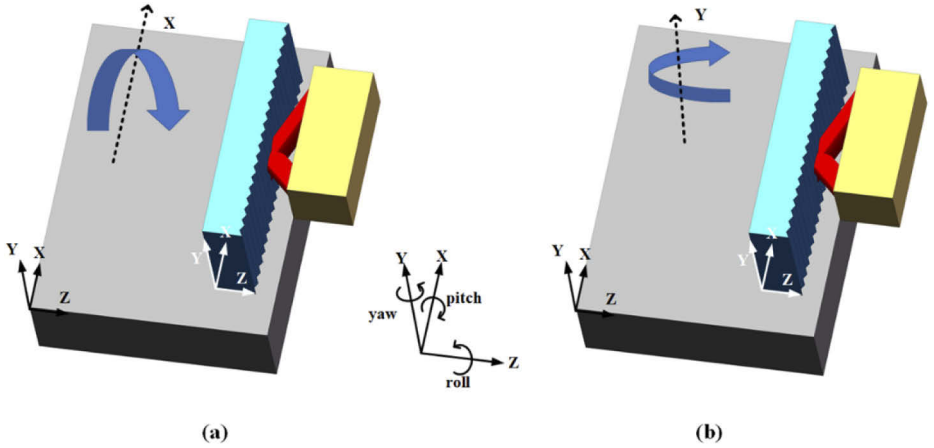

Fig. 6. Workbench errors: (a) pitch (b) yaw.

Table 2. Influence of the polar and azimuthal angles of incidence on displacement for various groove conditions.

Grating type	Azimuthal angle Phase change (rad)	Azimuthal angle Displacement change (nm)	Polar angle Phase change (rad)	Polar angle Displacement change (nm)
Binary	0.0112	0.2483	0.0256	0.5656
Sinusoidal	0.0016	0.0356	0.0206	0.4553
Triangular	0.0011	0.0252	0.0199	0.4398
Trapezoidal	0.0129	0.2852	0.0201	0.4441

4. Experiment

4.1. Experiment setup

In the setup, (Fig. 7), a dual-frequency laser operating at a wavelength of 632.8 nm and a frequency difference of 2.4 MHz is used as the light source. The setup includes a motorized linear stage (XML210-S, Newport), the grating, and two mirrors aligned to the grating at a polar angle of 45° and an azimuth angle of 45°. The grating is an 1800gr/mm planar holographic grating with a trapezoidal groove of size 50 mm × 25 mm × 10 mm. The point of incidence is located at the longitudinal center of the grating; its diameter is 3 mm. Two plane mirrors with vertical reflecting surfaces are set on the ±1 diffraction line, and a cable of signal receiver is set on the other side of the PBS. As a reference, a laser interferometer (LI) from Keysight is used to provide standard displacement data, and use a reflective mirror as measuring mirror (Mirror-LI).

After completing the setup, the diffraction efficiency of the measurement system is tested, and the energy of the total incident light, P-polarized light, S-polarized light, P-polarized diffraction light and S-polarized diffraction light is measured (see Table 3).

Due to double diffraction in measuring path, it is difficult to measure each P-/S-polarized light energy in diffraction path. We define the equivalent diffraction efficiency as the ratio of the P-/S-polarized energy at receiver and the P-/S-polarized energy after PBS, our RCWA analysis and energy measurement all follow this definition. The equivalent diffraction efficiency of P-polarized light is 1.52%, and that of S-polarized light is 1.5% (from Table 3), which is consistent with the RCWA simulation results (see Fig. 3. and Fig. 4.).

Optics EXPRESS

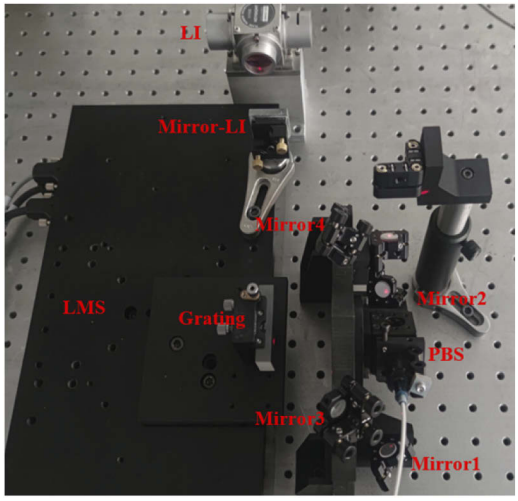

Fig. 7. Setup for the conical diffraction grating interferometer.

Table 3. Energy testing of the grating interferometer.

	Energy (μW)
Total incident energy	80
P-polarized light	38
S-polarized light	40
P-polarized diffraction light	0.58
S-polarized diffraction light	0.6

4.2. Displacement experiment

Taking into account the actual position of the spot on the grating surface, the actual range of motion is 43 mm, and multiple round-trip tests of the motion are carried out. The speed of the test is 1 mm/s, the time for a single round-trip is 43 s, and a 500-ms delay is set between each round-trip. The results are represented in Fig. 8.

For Abbe error [26], because of the standard data from laser interferometer, we use data from laser interferometer to decrease the data from grating interferometer, then fix the differences' slope. Next, we use the difference to decrease the data from the slope multiply the standard data. In this step, we remove the abbe error. The last difference we called residual error. The residual measurement error (Fig. 9(a)) after removing the Abbe error is obtained from repeated measurement data yielding an error of 200 nm (3σ). However, the repeatability of multiple measurement results after removing the Abbe error remains the same. From our previous work [27], the main source of error stems from grating processing, which is classified as systematic error. Therefore, the error is fitted and included as a compensation value in the displacement data.

The error obtained from the repeatability study is fitted in accordance with the average interval of the segment, and then the curve after fitting is compared with the original residual error, red line in Fig. 9(b). The residual error after subtracting the fitting (Fig. 10(a)) has a standard error of 33nm (3σ). The error stems from workbench vibration and disturbances in the environment. In Fig. 10(b)., we do experiment going forward and going backward, and use fit curve in Fig. 9(b). to correct, so there are two displacement error matching with on laser interferometer data. The repeated residual error (see Fig. 10(b)) is 45 nm (3σ).

Optics EXPRESS

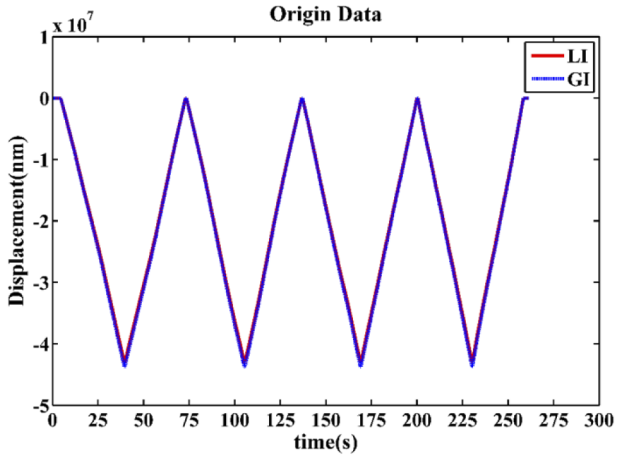

Fig. 8. Displacement test.

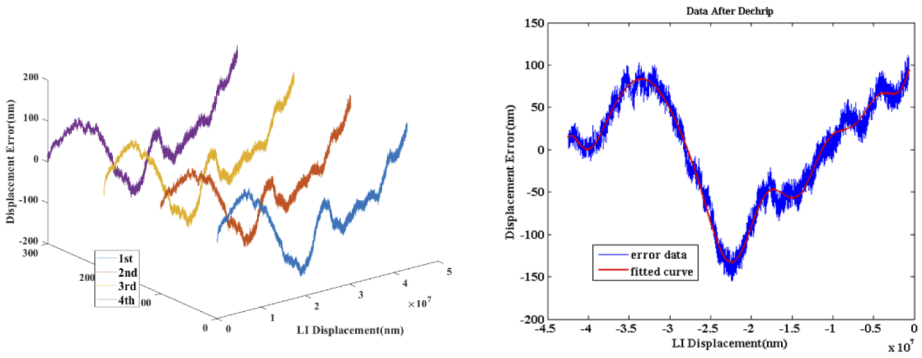

Fig. 9. (a) Repeatability testing and (b) fitted curve of the displacement data.

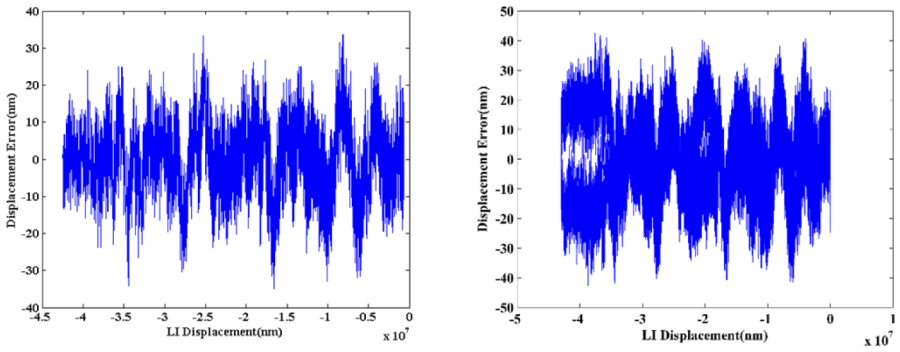

Fig. 10. (a) Residual error and (b) repeated residual error for the displacement error.

Optics EXPRESS

5. Conclusion

The conical diffraction grating interferometer proposed in this paper uses a grating to modulate the polarization, so that the polarization state of incident pure-polarized light is changed. The light is then split by a PBS to enable interferometry to be performed. The measurement error incurred from processing and installing of a QWP is reduced. A mirror is used to reflect the diffracted light vertically to realize a second diffraction, which improves the optical subdivision ratio and ensures a more precise optical path. RCWA is used to analyze the P- and S-polarization components in the interference signal. For different grating types, the energy for S-polarization is consistent with that for P-polarization and is also consistent when installation errors of the optical elements are taken into account. Because of the change in polarization state, the phase of the beam also changes. This change in phase affects in turn the measurement error. Through our analysis, for incidence azimuthal and polar angles of 1°, the phase change incurred by the change in angle is 0.01 rad and 0.02 rad, respectively; the change in displacement is 0.23 nm and 0.45 nm. A conical diffraction grating interferometer was built and tested. Its range in measurement is 43 mm. An analysis of the measurement results showed good repeatability for the measurement system. After removing the repeatability error, the random error is 45 nm. After correction, the conical diffraction grating interferometer displays good repeatability and good measurement accuracy.

Funding. Strategic Priority Research Program of the Chinese Academy of Sciences (XDC04000000); R & D projects in key areas of Guangdong Province (2019B010144001); National Natural Science Foundation of China (61905245); Jilin Province Science & Technology Development Program Project in China (20190303019SF, 20200401071GX).

Disclosures. The authors declare no conflicts of interest.

Data availability. Data underlying the results presented in this paper are not publicly available at this time but may be obtained from the authors upon reasonable request.

References

1. G. H. Yuan and N. I. Zheludev, "Detecting nanometric displacements with optical ruler metrology," Science **364**(6442), 771–775 (2019).
2. T. Castenmiller, F. van de Mast, T. de Kort, C. van de Vin, M. de Wit, R. Stegen, and S. van Cleef, "Towards ultimate optical lithography with nxt: 1950i dual stage immersion platform," in Optical Microlithography XXIII,vol. 7640(International Society for Optics and Photonics, 2010), p. 76401N.
3. Z. Xiong, H. Liu, X. Tan, Z. Lu, C. Li, L. Song, and Z. Wang, "Diffraction analysis of digital micromirror device in maskless photolithography system," J. Micro/Nanolith. MEMS MOEMS **13**(4), 043016 (2014).
4. Y. Zhang, J. Luo, Z. Xiong, H. Liu, L. Wang, Y. Gu, Z. Lu, J. Li, and J. Huang, "User-defined microstructures array fabricated by dmd based multistep lithography with dose modulation," Opt. Express **27**(22), 31956–31966 (2019).
5. Z. Xiong, P. Kunwar, and P. Soman, "Hydrogel-based diffractive optical elements (hdoes) using rapid digital photopatterning," Adv. Opt. Mater. **9**(2), 2001217 (2021).
6. S. Guo, Z. Lu, Z. Xiong, L. Huang, H. Liu, and J. Li, "Lithographic pattern quality enhancement of dmd lithography with spatiotemporal modulated technology," Opt. Lett. **46**(6), 1377–1380 (2021).
7. Z. Xiong, H. Liu, R. Chen, J. Xu, Q. Li, J. Li, and W. Zhang, "Illumination uniformity improvement in digital micromirror device based scanning photolithography system," Opt. Express **26**(14), 18597–18607 (2018).
8. P. Kunwar, A. V. S. Jannini, Z. Xiong, M. J. Ransbottom, J. S. Perkins, J. H. Henderson, J. M. Hasenwinkel, and P. Soman, "High-resolution 3d printing of stretchable hydrogel structures using optical projection lithography," ACS Appl. Mater. Interfaces **12**(1), 1640–1649 (2020).
9. C.-F. Kao, S.-H. Lu, H.-M. Shen, and K.-C. Fan, "Diffractive laser encoder with a grating in Littrow configuration," Jpn. J. Appl. Phys. **47**(3), 1833–1837 (2008).
10. Q. Lv, Z. Liu, W. Wang, X. Li, S. Li, Y. Song, H. Yu, Bayanheshig, and W. Li, "Simple and compact grating-based heterodyne interferometer with the Littrow configuration for high-accuracy and long-range measurement of two-dimensional displacement," Appl. optics **57**(31), 9455–9463 (2018).
11. H. Hsieh, J. Lee, W. Wu, J. Chen, R. Deturche, and G. Lerondel, "Quasi-common-optical-path heterodyne grating interferometer for displacement measurement," Meas. Sci. Technol. **21**(11), 115304 (2010).
12. J. Deng, X. Yan, C. Wei, Y. Lu, M. Li, X. Xiang, W. Jia, and C. Zhou, "Eightfold optical encoder with high-density grating," Appl. optics **57**(10), 2366–2375 (2018).
13. D. Chang, X. Xing, P. Hu, J. Wang, and J. Tan, "Double-diffracted spatially separated heterodyne grating interferometer and analysis on its alignment tolerance," Appl. Sci. **9**(2), 263 (2019).

Optics EXPRESS

14. W. Ye, M. Zhang, Y. Zhu, L. Wang, J. Hu, X. Li, and C. Hu, "Translational displacement computational algorithm of the grating interferometer without geometric error for the wafer stage in a photolithography scanner," Opt. Express **26**(26), 34734–34752 (2018).
15. W. Ye, M. Zhang, Y. Zhu, L. Wang, J. Hu, X. Li, and C. Hu, "Ultraprecision real-time displacements calculation algorithm for the grating interferometer system," Sensors **19**(10), 2409 (2019).
16. F. Yang, M. Zhang, Y. Zhu, W. Ye, L. Wang, and Y. Xia, "Two degree-of-freedom fiber-coupled heterodyne grating interferometer with milli-radian operating range of rotation," Sensors **19**(14), 3219 (2019).
17. L. Šiaudinyte, G. Molnar, R. Köning, and J. Flügge, "Multi-dimensional grating interferometer based on fibre-fed measurement heads arranged in Littrow configuration," Meas. Sci. Technol. **29**(5), 054007 (2018).
18. X. Li, W. Gao, H. Muto, Y. Shimizu, S. Ito, and S. Dian, "A six-degree-of-freedom surface encoder for precision positioning of a planar motion stage," Precis. Eng. **37**(3), 771–781 (2013).
19. A. Kimura, W. Gao, W. Kim, K. Hosono, Y. Shimizu, L. Shi, and L. Zeng, "A sub-nanometric three-axis surface encoder with short-period planar gratings for stage motion measurement," Precis engineering **36**, 576–585 (2012).
20. H. Fu, Y. Wang, P. Hu, J. Tan, and Z. Fan, "Nonlinear errors resulting from ghost reflection and its coupling with optical mixing in heterodyne laser interferometers," Sensors **18**(3), 758 (2018).
21. J. Cui, Z. He, J. Tan, and T. Sun, "Realization of a robust homodyne quadrature laser interferometer by performing wave plate yawing to realize ultra-low error sensitivity," Opt. Express **24**(20), 23505–23518 (2016).
22. H. Lochbihler, "Diffraction from highly conducting lamellar gratings in conical mountings," J. Mod. Opt. **43**(9), 1867–1890 (1996).
23. D. Wei, H. Liu, M. Cao, R. Liu, L. Han, P. Zhang, Y. Zhou, H. Li, H. Gao, and F. Li, "Polarization separation of light in holographic grating reflection in conical mounting," J. Mod. Opt. **60**(7), 598–601 (2013).
24. M. Moharam, E. Grann, D. Pommet, and T. Gaylor, "Formulation for stable and efficient implementation of the rigorous coupled-wave analysis of binary gratings," J. Opt. Soc. Am. A **12**(5), 1068–1076 (1995).
25. P. Kwiecien and I. Richter, "Modeling of plasmonic nanostructures using efficient three dimensional aperiodic rigorous coupled wave analysis," in Laser Science, (Optical Society of America, 2011), p. JWA41.
26. M. H. G. Khouygani and J.-Y. Jeng, "High-precision miniaturized low-cost reflective grating laser encoder with nanometric accuracy," Appl. Opt. **59**(19), 5764–5771 (2020).
27. Q. Lv, Z. Liu, W. Wang, S. Jiang, W. Bayanheshig, and Li, "Fast method to detect and calculate displacement errors in a littrow grating-based interferometer," Appl. Opt. **58**(12), 3193–3199 (2019).